Ultra-low reflection porous silicon nanowires for solar cell applications

Adel Najar, Joël Charrier, Parastesh Pirasteh, R. Sougrat

Ultra-low reflection porous silicon nanowires for solar cell applications

A. Najar,[1,*] J. Charrier,[2] P. Pirasteh,[2] and R. Sougrat[3]

[1]*King Abdullah University of Science and Technology (KAUST), Saudi Arabia*
[2]*Universite europeenne de Bretagne, CNRS FOTON, UMR 6082, ENSSAT BP80518, F-22305 Lannion Cedex, France*
[3]*Advanced Nanofabrication, Imaging and Characterization Core Facilities, King Abdullah University of Science and Technology (KAUST), Saudi Arabia*
[*]*najar.adel@laposte.net*

Abstract: High density vertically aligned Porous Silicon NanoWires (PSiNWs) were fabricated on silicon substrate using metal assisted chemical etching process. A linear dependency of nanowire length to the etching time was obtained and the change in the growth rate of PSiNWs by increasing etching durations was shown. A typical 2D bright-field TEM image used for volume reconstruction of the sample shows the pores size varying from 10 to 50 nm. Furthermore, reflectivity measurements show that the 35% reflectivity of the starting silicon wafer drops to 0.1%, recorded for more than 10 μm long PSiNWs. Models based on cone shape of nanowires located in a circular and rectangular bases were used to calculate the reflectance employing the Transfert Matrix Formalism (TMF) of the PSiNWs layer. Using TMF, the Bruggeman model was used to calculate the refractive index of PSiNWs layer. The calculated reflectance using circular cone shape fits better the measured reflectance for PSiNWs. The remarkable decrease in optical reflectivity indicates that PSiNWs is a good antireflective layer and have a great potential to be utilized in radial or coaxial p-n heterojunction solar cells that could provide orthogonal photon absorption and enhanced carrier collection.

OCIS codes: (310.1210) Thin films; (310.1860) Thin films; (040.5350) Detectors.

References and links

1. L. Tsakalakos, "Nanostructures for photovoltaics," Mater. Sci. Eng. **62**(6), 175–189 (2008).
2. N. S. Lewis, "Toward cost-effective solar energy use," Science **315**(5813), 798–801 (2007).
3. P. Lalanne and G. M. Morris, "Design, fabrication and characterization of subwavelength periodic structures for semiconductor anti-reflection coating in the visible domain," Proc. SPIE **2776**, 300–309 (1996).
4. T. L. Canham, "Silicon quantum wire array fabrication by electrochemical and chemical dissolution of wafers," Appl. Phys. Lett. **57**(10), 1046–1048 (1990).
5. A. Najar, J. Charrier, H. Ajlani, N. Lorrain, S. Haesaert, M. Oueslati, and L. Haji, "Optical gain at 1.53 μm in Er^{3+}-Yb^{3+} co-doped porous silicon waveguides," Mater. Sci. Eng. B **146**(1-3), 260–263 (2008).
6. A. Najar, J. Charrier, N. Lorrain, L. Haji, and M. Oueslati, "Optical gain measurements in porous silicon planar waveguides codoped by erbium and ytterbium ions at 1.53 μm," Appl. Phys. Lett. **91**(12), 121120 (2007).
7. S. Yae, T. Kobayashi, T. Kawagishi, N. Fukumuro, and H. Matsuda, "Antireflective porous layer formation on multicrystalline silicon by metal particle enhanced HF etching," Sol. Energy **80**(6), 701–706 (2006).
8. P. Vitanov, M. Kamenova, N. Tyutyundzhiev, M. Delibasheva, E. Goranova, and M. Peneva, "High-efficiency solar cell using a thin porous silicon layer," Thin Solid Films **297**(1-2), 299–303 (1997).
9. K. Ueda, Y. Nakato, and H. Tsubomura, "Efficient and stable solar to chemical conversion with n+-p junction crystalline silicon electrodes having textured surfaces," Sol. Energy Mater. **17**(1), 37–46 (1988).
10. K. Q. Peng, Y. Xu, Y. Wu, Y. J. Yan, S. T. Lee, and J. Zhu, "Aligned single-crystalline Si nanowire arrays for photovoltaic applications," Small **1**(11), 1062–1067 (2005).
11. O. L. Muskens, J. G. Rivas, R. E. Algra, E. P. Bakkers, and A. Lagendijk, "Design of light scattering in nanowire materials for photovoltaic applications," Nano Lett. **8**(9), 2638–2642 (2008).
12. T. Stelzner, M. Pietsch, G. Andrä, F. Falk, E. Ose, and S. Christiansen, "Silicon nanowire-based solar cells," Nanotechnology **19**(29), 295203 (2008).
13. V. Sivakov, G. Andrä, A. Gawlik, A. Berger, J. Plentz, F. Falk, and S. H. Christiansen, "Silicon nanowire-based solar cells on glass: synthesis, optical properties, and cell parameters," Nano Lett. **9**(4), 1549–1554 (2009).

#164877 - $15.00 USD Received 19 Mar 2012; revised 22 May 2012; accepted 23 May 2012; published 11 Jul 2012

14. B. M. Kayes, H. A. Atwater, and N. S. Lewis, "Comparison of the device physics principles of planar and radial p-n junction nanorod solar cells," J. Appl. Phys. **97**(11), 114302 (2005).
15. B. Z. Tian, X. L. Zheng, T. J. Kempa, Y. Fang, N. F. Yu, G. H. Yu, J. L. Huang, and C. M. Lieber, "Coaxial silicon nanowires as solar cells and nanoelectronic power sources," Nature **449**(7164), 885–889 (2007).
16. E. C. Garnett and P. D. Yang, "Silicon nanowire radial p-n junction solar cells," J. Am. Chem. Soc. **130**(29), 9224–9225 (2008).
17. L. Tsakalakos, J. Balch, J. Fronheiser, B. A. Korevaar, O. Sulima, and J. Rand, "Silicon nanowire solar cells," Appl. Phys. Lett. **91**(23), 233117 (2007).
18. L. Hu and G. Chen, "Analysis of optical absorption in silicon nanowire arrays for photovoltaic applications," Nano Lett. **7**(11), 3249–3252 (2007).
19. L. J. Lauhon, M. S. Gudiksen, D. Wang, and C. M. Lieber, "Epitaxial core-shell and core-multishell nanowire heterostructures," Nature **420**(6911), 57–61 (2002).
20. M. Law, J. Goldberger, and P. D. Yang, "Semiconductor nanowires and nanotubes," Annu. Rev. Mater. Res. **34**(1), 83–122 (2004).
21. A. I. Hochbaum, D. Gargas, Y. J. Hwang, and P. D. Yang, "Single crystalline mesoporous silicon nanowires," Nano Lett. **9**(10), 3550–3554 (2009).
22. A. Najar, A. B. Slimane, M. N. Hedhili, D. H. Anjum, T. K. Ng and Boon S. Ooi, "Structural and optical properties of porous silicon nanowires prepared by metal-assisted electroless etching method - effect of HF concentration," J. of Appl. Phys., (2012). (under reviewing)
23. D. E. Aspnes, "Optical properties of thin films," Thin Solid Films **89**(3), 249–262 (1982).
24. W. Theiss, "Optical properties of porous silicon," Surf. Sci. Reports 29 91–93 and 95–192 (1997).
25. T.-H. Pei, S. Thiyagu, and Z. Pei, "Ultra high-density silicon nanowires for extremely low reflection in visible regime," Appl. Phys. Lett. **99**(15), 153108 (2011).
26. A. C. Diebold and J. Price, "Observation of quantum confinement and quantum size effects," Phys. Status Solidi **205**(4), 896–900 (2008) (a).

1. Introduction

Semiconductor nanostructures are promising building blocks for next generation solar cells with higher energy conversion efficiencies and lower cost [1,2]. Silicon-based nanostructured solar cells have several advantages, including the natural abundance of silicon, lack of toxicity, and compatibility with mature integrated-circuit fabrication techniques. In order to improve light harvesting in solar cells, it is mandatory to minimize the Fresnel reflection at the air/ silicon interface for the range of the entire solar spectrum. In the past, a multilayer antireflection coating (ARC) was commonly used to reduce surface reflection. However, issues related to material selection, thermal mismatch, and instability of the thin-film stacks remained major obstacles to the application of such broadband and angle-independent antireflection coatings in solar cells [3].

A porous silicon (PS) layer formed on a crystalline silicon (c-Si) wafer using electrochemical etching exhibits photoluminescent and electroluminescent properties similar to those of semiconductors with a direct energy band gap [4–6]. The main improvement in the performance of the PS layers is the rough surface and low effective refractive index compared with c-Si, which can decrease the reflective loss of solar radiation and lead to an increase of the short-circuit current density of solar cells [7–9]. Recently, vertically-aligned Silicon Nanowires (SiNWs) arrays exhibit low reflection and strong broadband absorption [10,11] and may be used as antireflection coatings or as the active layer in solar cells [10,12,13]. In particular, silicon nanowire arrays incorporating radial p-n junctions provide advantageous optoelectronic properties [14,15] that relax silicon quality requirement, enabling lower-cost cells. Several groups have demonstrated solar cells based on radial p-n junction SiNW arrays on different substrates [16,17]. Optical properties of SiNW arrays over the solar spectrum have previously been calculated [18]. They studied arrays with varying nanowire diameters for a fixed lattice constant of 100 nm, typical of the structures reported in Refs [19,20]. Their results showed that SiNW arrays could have much lower reflectance than silicon thin films. However, the overall absorption efficiencies of SiNW arrays were inferior to a silicon thin film of the same thickness. Recently, Porous Silicon Nanowires (PSiNWs), a nanostructure having mesopores carved into nanowires, were prepared by metal-assisted chemical etching method [21,22]. PSiNWs combine the physical properties of SiNWs and porous silicon is promising for solar cells, energy harvesting applications, and basic components for future nano-electronic, catalysis, and conversion.

#164877 - $15.00 USD Received 19 Mar 2012; revised 22 May 2012; accepted 23 May 2012; published 11 Jul 2012

In order to design optimal solar cells based on PSiNWs structures, theoretical investigation of their optical properties is needed to guiding further solar cell development. In particular, it is of interest to investigate the optical properties, including reflectance for different length of PSiNWs structures based on TMF (Transfert Matrix Formalism) and Bruggeman model.

2. Experimental conditions

PSiNWs were fabricated by Ag assisted electroless etching method from an n-type Si wafer (100) with a resistivity of 0.01-0.02 Ω-cm. The Si wafers were cleaned using acetone followed by ethanol for 5 minutes in an ultrasonic bath. Next, the wafers were immersed in a piranha solution H_2SO_4/H_2O_2 = (3:1) for 20 minutes to remove the organic deposits from the surface. The cleaned wafers were transferred into $HF/AgNO_3$ solution with a concentration of 4.8 M/0.005 M for Ag-deposition, followed by rinsing with de-ionized water to remove extra silver ions. Then, the Si samples were etched in the HF 4.8M/0.5M H_2O_2 solution for different times. At the end, samples were rinsed again for 10 minutes with HNO_3 solution to dissolve the Ag metal nanoparticles (NPs).

The surface morphology of PSiNWs was investigated using a FEI's Magellan 400 FEG SEM operating at 30 keV beam energy. The crystal structure, size of Si crystallites, and the average pore size were measured using the FEI's TitanG2 80-300 TEM. X-ray energy-dispersive spectroscopy (EDS) analysis of PSiNWs was carried out with an X-ray detector from EDAX (EDAX, Mahwah, NJ) attached to the TEM. Energy filtered TEM (EFTEM) was also performed to separate the crystalline phase of Si from its amorphous oxide phase using a GIF TridiemTM post-column energy filter from Gatan.

The reflectance spectra of the material were studied by a LAMBDA 900 Perkin-Elmer beam spectrometer equipped with a specular reflectance module with a 6° fixed angle. The effective refractive indices of the propagation modes in the planar waveguide were measured with a Metricon-2010 instrument. A laser beam at wavelengths 1540 nm is launched through a rutile prism into the film. As usual, from these measurements by the m-lines technique, the refractive indices and the thicknesses were deduced. This technique can be used to measure thickness and index for one or both films of a single or dual film structure.

3. Results and discussion

Figure 1(a) shows the scanning electron microcopy image of the vertically oriented PSiNWs having an average length of 13 μm after 75 min wet etching. The nanowires distribute uniformly on the sample. Figure 1(b) shows the top view with tips of NWs congregates together and the diameter of the congregated bundles is several micrometers. These congregated bundles are uniformly distributed on the entire samples and confirmed from the cross-section images. The transmission electron microscopy (TEM) image of an individual nanowire is shown Fig. 1(c), which shows that the nanowire has a diameter of ~150 nm. Most interestingly, the bright-field (BF) TEM micrograph in the inset in Fig. 1(c) reveals a dense distribution of pores on the surface of the nanowire. The FFT in the inset of Fig. 1(c) indicates the nanowires is single crystalline. Figure 1(d) shows the length of the NWs versus the etching time. The length of PSiNWs is linear as a function of the etching time up to 190 min with an etching rate of 0.12 $\mu m.min^{-1}$. This clearly indicates the rapidity of the electroless etching process. On the other hand, beyond 190 min, again revealed a linear relationship, with a change in the etching rate of the nanowires lower than the expected for 460 min etching time. The etching rate of the nanowires between 190 and 460 was 0.01 $\mu m.min^{-1}$. This clearly indicates that the reaction slows down due to the decrease in the reaction kinetics. We attribute this to the inhibition of the sinking mechanism of Ag^+ ions to the bottom of the nanowire arrays, leading to a decrease in Ag^+ concentration. The drop in Ag concentration results in the deceleration of etching rate.

#164877 - $15.00 USD Received 19 Mar 2012; revised 22 May 2012; accepted 23 May 2012; published 11 Jul 2012

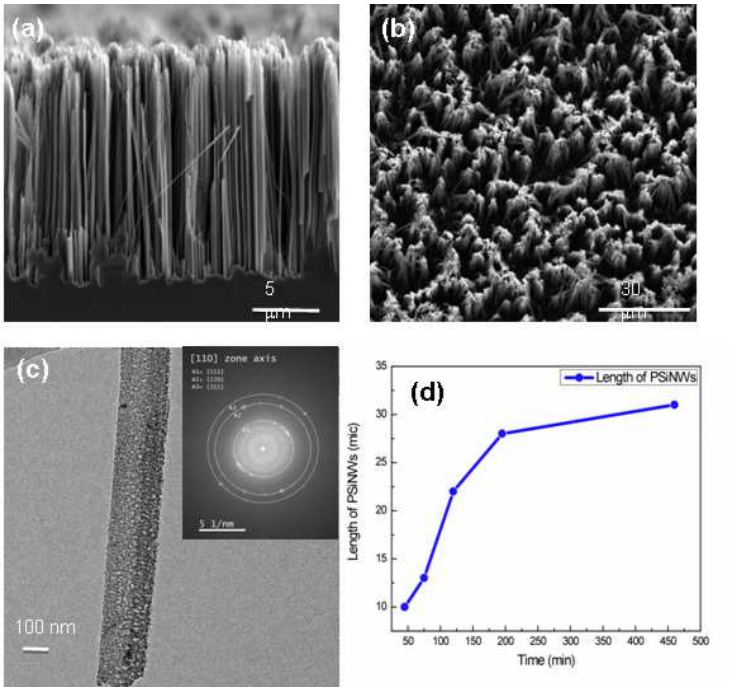

Fig. 1. (a) cross-section SEM micrograph of PSiNWs etched for 75 min, (b) top view micrograph of PSiNWs, (c) TEM image of individual nanowire and inset the FFT image, and (d) variation of the nanowires length as a function of etching time 45 min, 75 min, 120 min, 195 min and 460 min.

A typical 2D bright-field TEM image used for volume reconstruction of the sample is presented in Fig. 2. The three successive longitudinal slices obtained from the reconstructed volume revealed a distribution of irregular size/shape vacuum spaces and silicon frame, constituting the PSiNWs. The pores size is varying from 10 to 50 nm.

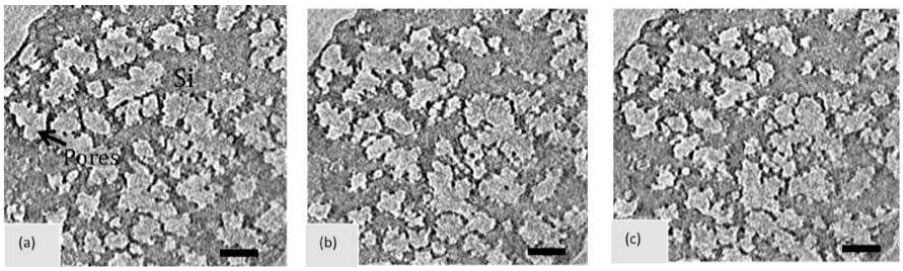

Fig. 2. (a), (b), and (c) represent three longitudinal slices extracted from the volume reconstruction of the PSiNW nanostructures revealing an area of highly porous medium. The bare scale is 50 nm.

4. Modeling and discussion

For modelling the reflectance spectrum of the PSiNWs layers, the refractive index of samples was measured at 1550 nm by m-lines technique. It was equal to 2.18 ± 0.2 whatever the used sample. By knowing this value and by using a classical model of effective media approximation, the Bruggeman effective medium approximation [23,24], the porosity of layer was deduced. For this purpose, a system composed of void pore embedded in a Si matrix was considered and the porosity was about of 48% ± 2. The evolution of the refractive index of sample was then calculated as a function of the wavelength (Fig. 3). Then the experimental spectra of PSiNW samples were measured for different thicknesses (10 µm, 13 µm, 28 µm,

#164877 - $15.00 USD Received 19 Mar 2012; revised 22 May 2012; accepted 23 May 2012; published 11 Jul 2012

and 31 µm) as shown in Fig. 4. These spectra reveal the low reflectance of PSiNW layers and permit to use these layers as anti-reflection coating of solar cells.

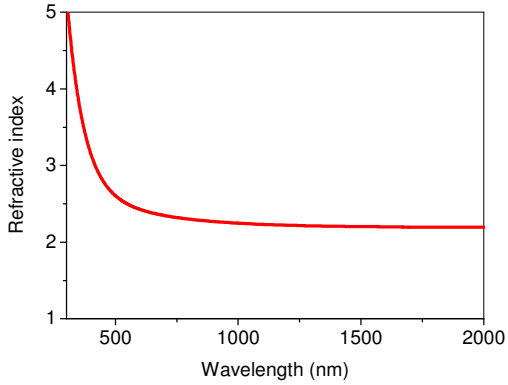

Fig. 3. Evolution of refractive index of SiNW layer as a function of the wavelength. The refractive index measured by m-lines at 1550 nm was equal to 2.18 ± 0.2 corresponding to a porosity of 48% by using Bruggeman model.

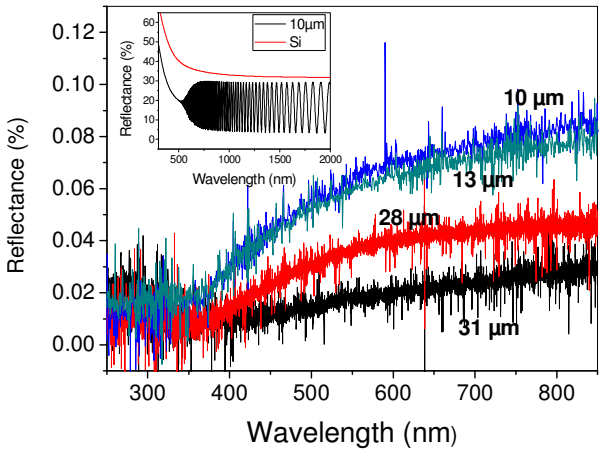

Fig. 4. Experimental spectra of PSiNW samples of different thickness (10 µm, 13 µm, 28 µm, and 31 µm). Inset: theoretical reflectance spectra of porous silicon layer (thickness equal to 10 µm) on Si substrate and Si substrate.

The generic structure under investigation is schematically depicted in Fig. 5. The PSiNWs were simulated by Si cones [25]. The z-axis is perpendicular to the Si substrate surface. The bottom of the PSiNW is at $z = 0$ and the top at $z = h$. The radius of the PSiNW depends on the z-position by the following equation $\rho = \frac{h - z}{h} R$ where R is the radius of the cone circle and h the thickness of layer. The PSiNW is divided into n horizontal layers with the same thickness denoted d equal to 1 nm. In the simulation model, each PSiNW is supposed to be located in a rectangular of egde equal to a or in a circle of diameter equal to a. According to the porosity value near of 50%, a is chosen as $2R$. This permits to simulate the reflectance for two different volume shape and to take the complex shape of PSiNWs into account.

#164877 - $15.00 USD Received 19 Mar 2012; revised 22 May 2012; accepted 23 May 2012; published 11 Jul 2012

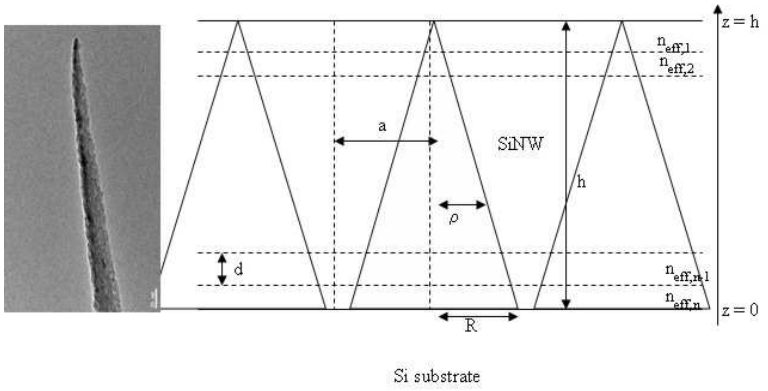

Fig. 5. Schematic representation of SiNWs and effective mulitlayer structure with cone shape and TEM image showing the cone shape.

Transfert Matrix Formalism (TMF) was applied to calculate the reflectance of electromagnic wave of through the multilayer structure simulating the PSiNWs layer (Fig. 5). In each zone, the wave-function is completely determined by two scalar components and can therefore be represented as a bi-dimensional (2D) column vector. The linearity of the Electromagnetism equations makes possible to relate the components between any two given abscissas z under a (2x2) matrix form. The transfer matrix of the whole structure is readily expressed as the matrix product:

$$[T] = \left[I_{air,n_{eff},1} \right] \left(\prod_{i=1}^{n-1} \left[M_{n_{eff},i} \right] \left[I_{n_{eff},i;n_{eff},i+1} \right] \right) \left[M_{n_{eff},n} \right] \left[I_{n_{eff},n;Si} \right]. \quad (1)$$

$$[T] = \begin{bmatrix} T_{11} & T_{12} \\ T_{21} & T_{22} \end{bmatrix}. \quad (2)$$

Where the notation (n_{eff}, i) corresponds to the i horizontal layer with the n_{eff} refractive index. $\left[I_{i;i+1} \right]$ is the matrix corresponding to the waves propagation across the interface between i and $i+1$ media and $\left[M_i \right]$ is the propagation matrix in the i medium according to Fig. 5.

Reflectance is given by the above equation.

$$R_{PSiNW} = \left| \frac{T_{21}}{T_{11}} \right|^2. \quad (3)$$

With this TMF, the Bruggeman model was used to calculate the refractive index of PSiNWs layer. From the Bruggeman model [23], knowing the volume fraction of Si and void, the refractive index of PSiNWs layer was deduced. This model takes into account the two media of the PSiNWs material according to the following equation:

$$f_{Si} \frac{\varepsilon_{Si} - \varepsilon}{\varepsilon_{Si} + 2\varepsilon} + f_{air} \frac{\varepsilon_{air} - \varepsilon}{\varepsilon_{air} + 2\varepsilon} = 0. \quad (4)$$

where ε_{Si}, ε_{air} and ε are the dielectric constants of silicon, air and PSiNWs layer respectively; f_{Si} and f_{air} are the weighting coefficients and $f_{Si} + f_{air} = 1$ with $\varepsilon_i = n_i^2$ where ni is the complex refractive index of Si or air.

#164877 - $15.00 USD Received 19 Mar 2012; revised 22 May 2012; accepted 23 May 2012; published 11 Jul 2012

The refractive index of bulk silicon is used in the Bruggeman model without considering the confinement effects of silicon nanostructures on the refractive index [26]. The aim of this modeling is to show the principal trends of reflectance evolution as a function of the SiNW length and the chosen base between circular and rectangular to explain experimental values of reflectance.

Lastly, $f_{Si,j} = \frac{\pi\rho^2}{a^2}$ or $f_{Si,j} = \frac{\pi\rho^2}{\pi(a/2)^2}$ respectively if the SiNW is located in a rectangular or a circle and $f_{air,j} = 1 - f_{Si,j}$ according to Fig. 5.

Firstly, the reflectance spectrum is calculated from TMF for a porous silicon layer with 50% porosity and a thickness equal to 10 µm on Si substrate layer in order to compare the reflectance spectra between PSi layer and PSiNW layer with the same porosity. Classical interfering fringes of the PSi layer and reflectance spectrum of Si substrate are observed in inset of Fig. 4 and the reflectance value is inferior to that of Si substrate. The comparison between the spectra of PSi and PSiNW layers shows the low obtained reflectance of PSiNW to use this layer as anti-reflection coating of solar cells.

Figures 6(a) and 6(b) and Fig. 7(a) and 7(b) show theoretical reflectance spectra of PSiNWs on silicon substrate for different layer thicknesses (0.5, 1, 5 and 10 µm) by considering cone shape according to Fig. 5 in the case where the PSiNW is located in a circle of radius equal to R or in a rectangle of edge equal to 2R. The reflectance of PSiNWs is strongly lower than that of porous silicon layer and the interfering fringes have low amplitudes notably on the case where the PSiNW is located in a circle. The constructive interference disappears when the thickness increases. Whatever the considered base, the reflectance decreases when the thickness of Si increases. The rectangular base permits to take into the porosity between the PSiNW account. The circular base permits to enhance artificially the porosity to take into the porosity between the SiNW and the porosity of the SiNW account. Figure 6(c) and 7(c) show the evolution of the porosity as a function of thickness by using cone shape according to different thickness of layers. The porosity drops with the increasing in layer thickness because of the shape of SiNW. Indeed, the width of PSiNW increases with the thickness so the porosity decreases. The porosity is more important in the case of the circular base. This permits to better simulate the reflectance spectrum of PSiNW layer by taking the porosity between the nanowires and the porosity of each nanowire into account. The fringes also disappear and the reflectance drops brutally for the low wavelengths due to the strong absorption of the silicon material in the simulations as we can also see in the inset in Fig. 4 for the case of porous silicon layer.

#164877 - $15.00 USD Received 19 Mar 2012; revised 22 May 2012; accepted 23 May 2012; published 11 Jul 2012

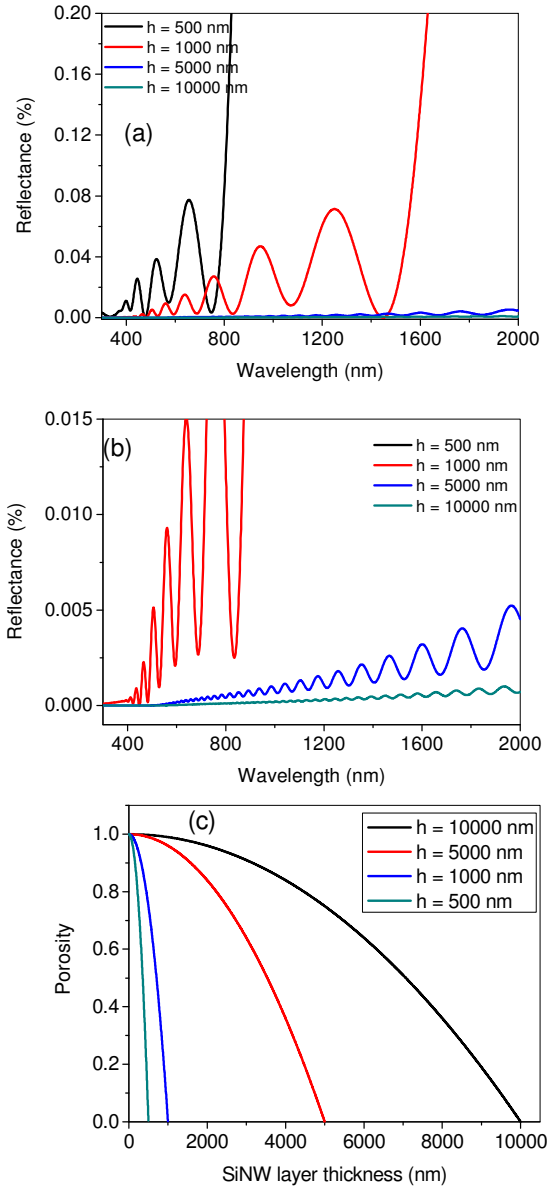

Fig. 6. (a) Theoretical reflectance spectra of SiNWs on silicon substrate for different layer thicknesses (0.5, 1, 5 and 10 µm) by considering cone shape and circular base, (b) Zoom of theoretical reflectance spectra of SiNWs, (c) Evolution of porosity as a function of thickness by using cone shape and circular base.

#164877 - $15.00 USD Received 19 Mar 2012; revised 22 May 2012; accepted 23 May 2012; published 11 Jul 2012

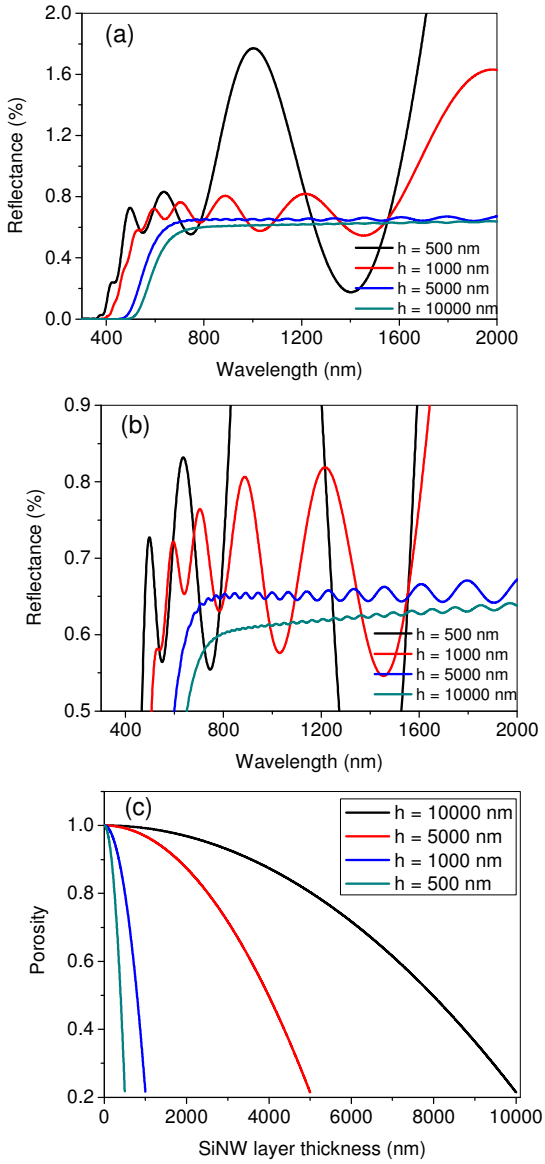

Fig. 7. (a) Theoretical reflectance spectra of SiNWs on silicon substrate for different layer thicknesses (0.5, 1, 5 and 10 µm) by considering cone shape and rectangular base, (b) Zoom of theoretical reflectance spectra of SiNWs, (c) Evolution of porosity as a function of thickness by using cone shape and rectangular base.

Figure 8 represents experimental and theoretical reflectance spectra of PSiNWs on silicon substrate corresponding to different samples with their thickness by considering cone shape. The interferences are clearly observed in the calculated reflectance for the low lengths of PSiNWs whereas the experimental reflectance shows no interference. However, the same trends are observed on experimental and theoretical spectra: the experimental value of reflectance is between those obtained by the two models. The reflectance decreases strongly for the low wavelength and increases slightly towards the higher wavelengths. According to the used model, the porosity is majored or minored with a circle base or rectangular base respectively that is why the reflectance values are different.

#164877 - $15.00 USD Received 19 Mar 2012; revised 22 May 2012; accepted 23 May 2012; published 11 Jul 2012

In the Bruggeman effective medium approximation model, we do not take into account the fraction of SiO_2 on the nanowires surface and the congregate and bundles of nanowires. For these reasons we have a small difference between the theoretical and experimental spectra. So the experimental reflectance appears as the pondered sum between the two theoretical reflectance spectra due to the PSiNW complex shape.

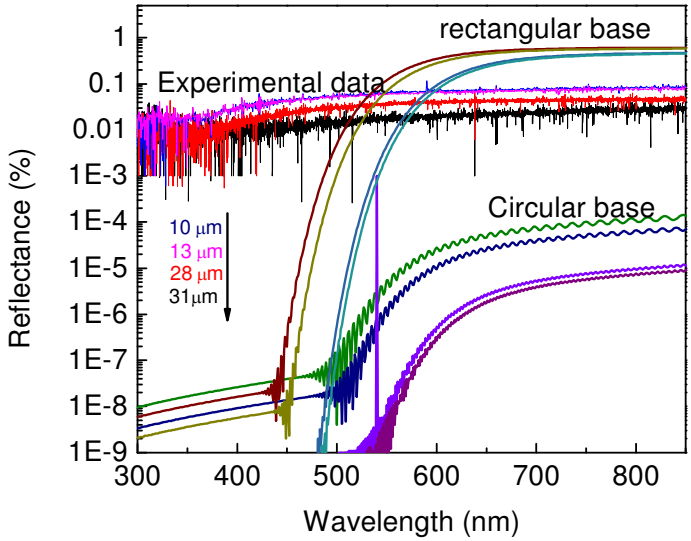

Fig. 8. Experimental reflectance spectra and theoretical reflectance spectra using the conic model with circular base and rectangular base for the different thicknesses of samples (10 μm, 13 μm, 28 μm, and 31 μm).

In summary, high density and high length PSiNWs exhibiting extremely low reflectanve over a wavelength range from 400 to 850 nm were elaborated. The average reflectance varies from 0.04 to 0.2% for this wavelength range.

5. Conclusion

We have fabricated large-area of porous silicon nanowire by Ag assisted electroless etching method. A linear dependency of nanowires length was obtained and the change in growth rate for long etching time was shown. 2D bright-field TEM image used for volume reconstruction of the sample shows pores size varying from 10 to 50 nm. Reflection measurements were carried out and the effect of length on the reflectivity were elaborated. The reflectivity of the samples decreased drastically compared to Si substrate, which kept on decreasing with a further increase in the nanowire length. A PSiNWs with 31 μm long was found to have the lowest reflectivity, 0.1%. A model based on circular cone shape of nanowires fits better the measured reflectance employing the Transfert Matrix Formalism of the PSiNWs layer. Finally, our work demonstrates the feasibility of the use of PSiNWs fabricated by the Ag assisted electroless etching method in heterojunction thin film solar cells with promising antireflective performance.

#164877 - $15.00 USD Received 19 Mar 2012; revised 22 May 2012; accepted 23 May 2012; published 11 Jul 2012